Volume 21
Number 3
21 January 2025
Pages 315–528

Soft Matter

rsc.li/soft-matter-journal

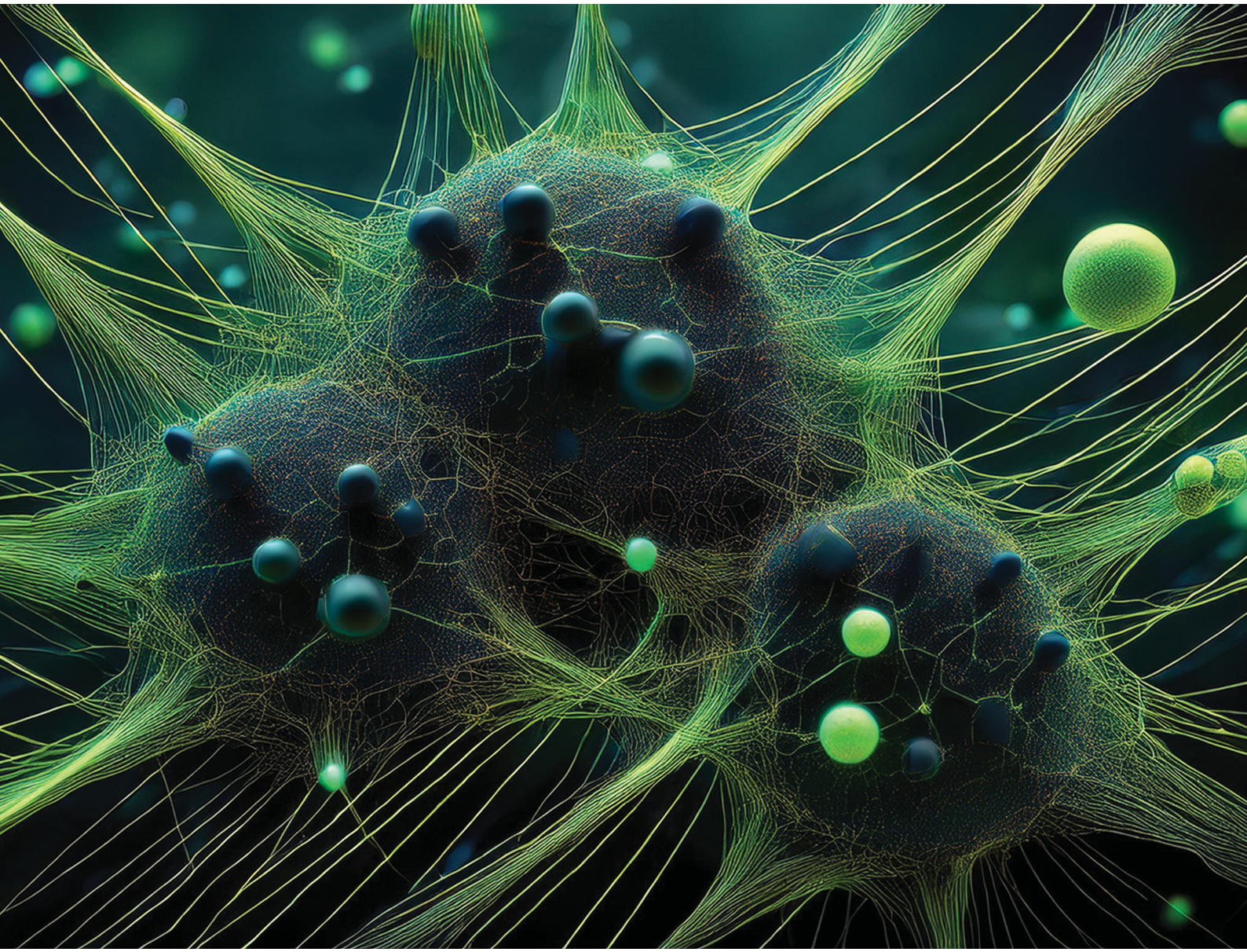

ISSN 1744-6848

ROYAL SOCIETY OF CHEMISTRY

COMMUNICATION
Guilhem P. Baeza *et al.*
Understanding polymer–colloid gels: a solvent perspective using low-field NMR

20 YEARS ANNIVERSARY

Soft Matter

COMMUNICATION

View Article Online
View Journal | View Issue

Check for updates

Cite this: *Soft Matter*, 2025, **21**, 342

Received 15th September 2024,
Accepted 3rd November 2024

DOI: 10.1039/d4sm01098a

rsc.li/soft-matter-journal

Published on 06 November 2024. Downloaded on 29/1/2026 11:08:33 AM.

Understanding polymer–colloid gels: a solvent perspective using low-field NMR†

Léo Hervéou,‡[ab] Gauthier Legrand,‡[b] Thibaut Divoux [b] and Guilhem P. Baeza §*[a]

The present work emphasizes the relevance of low-field NMR relaxometry to investigate colloid-polymer hydrogels by probing water dynamics across a wide range of formulations between 10 °C and 80 °C. By examining the temperature dependence of the transverse relaxation time T_2, we demonstrate a clear link between the NMR response and the rheological behavior of the hydrogels. In particular, we show that NMR relaxometry targeting the solvent provides reliable insights into the hydrogel microstructure and allows the detection of phase transitions and aging processes. Our findings suggest that this solvent-focused technique could greatly benefit the soft matter community, complementing other experimental methods in the study of gels.

Hydrogels represent a fascinating class of versatile materials originally consisting of a low fraction of hydrosoluble polymer forming a 3D percolated network in water.[1] Important progress regarding their structural design has been made in the last few decades, notably leading to the emergence of double-[2–4] and hybrid-networks,[5,6] respectively incorporating two (or more[7]) polymers and inorganic particles. These advanced materials exhibit enhanced mechanical properties, leading to widespread use in key sectors like the food industry,[8,9] medical engineering,[10–12] and energy.[13,14] Among them, natural polymer-based hydrogels relying on networks of proteins, polyesters, or polysaccharides present the advantage of employing abundant, biocompatible, and (sometimes) edible polymers. Their amphiphilic nature, coupled with well-chosen inorganic particles, results in a rich phase diagram where mechanical properties can be easily selected from the formulation and the processing conditions.[15–17] For example, we have recently demonstrated the dual nature of physical hydrogels made of the sodium salt of carboxymethylcellulose (CMC) and carbon black (CB) soot particles. Depending on their composition, CB–CMC hydrogels can either display a microstructure akin to a colloidal gel in which a percolated network of CB particles is stabilized by CMC, or a polymer gel in which a CMC matrix is physically cross-linked by CB particles.[18]

Besides, the amphiphilic character of natural polymer-based hydrogels makes them particularly thermo-sensitive, including within the narrow temperature window defined by water crystallization and vaporization (0 and 100 °C).[19] In addition to irreversible chemical alteration, temperature changes can significantly impact chain conformation (*e.g.*, protein denaturation)[20], or strongly influence the gelation scenario, leading to major topological changes of the network.[21] Such changes have been evidenced by multiple techniques, among which low-field (LF) NMR relaxometry was shown to yield precious insights regarding the microstructure of complex biological tissues[22,23] and foodstuff.[24–27] This technique, which is used to obtain information about the mobile protons of a sample, has also been recently coupled to rheometry offering time-resolved information on the sample microstructure under shear.[28–31] In solid porous media, low-field NMR targets the solvent to compute the sample's pore size distribution.[32] In contrast, in aqueous suspensions and hydrogels, where water is replaced by D_2O to mask the contribution from the proton of the solvent, low-field NMR targets the dynamics of the dispersed phase alone.

Here, we take a mixed approach by conducting LF ^{1}H-NMR experiments on CB–CMC hydrogels to monitor the dynamics of water, *i.e.*, the solvent, over a wide range of compositions and temperatures. The use of the popular Carr–Purcell–Meiboom–Gill (CPMG) pulse routine[33–35] allows us to measure the spin–spin (transverse) relaxation time T_2, which, in the case of pure water is of several seconds.[36] Our results clearly show that LF-NMR experiments targeting the solvent can effectively detect

[a] *INSA Lyon, UCBL, CNRS, MATEIS, UMR5510, 69621, Villeurbanne, France. E-mail: guilhem.baeza@insa-lyon.fr*
[b] *ENSL, CNRS, Laboratoire de physique, F-69342 Lyon, France*

† Electronic supplementary information (ESI) available: (1) $T_2 = f(c_{CMC})$ plots; (2) E_a values for all the samples; (3) cooling *vs.* heating $T_2 = f(1000/T)$ plots and E_a values for the whole set of samples; (4) corresponding viscous modulus of the elastic modulus plotted in Fig. 4; (5) CPMG experiments with various echo times. See DOI: https://doi.org/10.1039/d4sm01098a

‡ These authors contributed equally to this work.

§ Present address: Univ. Jean Monnet, Ingénierie des Matériaux Polymères, UMR 5223, 20 rue Annino, 42000 Saint-Etienne, France.

This journal is © The Royal Society of Chemistry 2025

Published on 06 November 2024. Downloaded on 29/1/2026 11:08:33 AM.

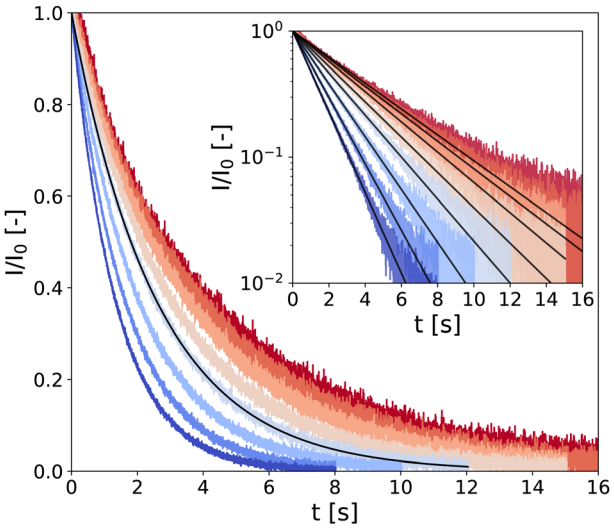

Fig. 1 LF-NMR CPMG signal normalized by I_0, the signal amplitude extrapolated at t = 0 s extracted from fitting the data with eqn (1) (black solid lines). Measurements are performed on a CMC0.01–CB2 hydrogel, every 10 °C between 10 °C and 80 °C (see color code from dark blue to red). Inset: Same data in semi-logarithmic representation.

the sol–gel transition, thermally-induced phase transition, and physical aging. This makes it a promising and complementary technique to the traditional focus on the dispersed phase.

In the following, samples are denoted through the code "CMC*X*-CB*Y*," where X and Y represent the mass fraction (in wt%) of CB and CMC, respectively (see technical details in the Experimental section). Typical CPMG experiment outputs are presented in Fig. 1 for a low-density gel, *i.e.*, a hydrogel of composition CMC0.01–CB2 where the transverse magnetization of hydrogen atoms (almost exclusively coming from water) $I(t)$ decreases over a characteristic time T_2 following the expression

$$I(t) = I_0 \exp(-t/T_2), \quad (1)$$

where $I_0 = I(0)$ and t is the experimental time. As expected, T_2 increases for higher temperatures, indicating the overall greater mobility of water molecules. However, in contrast to several other natural polymer-based hydrogels,[30,37–39] the single and unstretched character of the exponential decay suggests that, on average, over the entire experimental time, all water molecules in the hydrogel exhibit identical dynamics. In other words, despite the spatial density fluctuations and the corresponding various residence times in different microenvironments, water molecules appear to move through the material much faster than the time required to lose their magnetization. This indicates the absence of significant molecular immobilization, which might have been expected in hydrophilic polymers.[40–43] A rough estimate of the diffusion length L_D, calculated using the self-diffusion coefficient of water at room temperature[44] ($D_w \approx 2.3 \times 10^{-9}$ m^2 s^{-1}) and T_2 ($\approx$2 s), yields $L_D = \sqrt{D_w T_2} \approx 68$ mm. This value is significantly larger than the mesh size of CMC gels determined from rheometry, which is approximately 50 nm (ref. 45) and comparable to the average diameter of CMC fringe micelles measured by neutron scattering, approximately 75 nm.[46]

Fig. 2 gathers the times T_2 measured across all samples investigated between 10 and 80 °C. The first row highlights the impact of CB content (x_{CB} = 0–8 wt%) in three hydrogel matrices made of 0.01, 0.5, and 3 wt% of CMC, while the second row examines the impact of CMC concentration (c_{CMC} = 0.01–3 wt%) for three CB contents 2, 4, and 8 wt%. At first glance, T_2 generally decreases as the reciprocal temperature increases, reflecting the reduced mobility of water molecules. As expected, and consistent with our previous work on CMC hydrogels,[46] T_2 in CB-free samples follows an Arrhenius dependence across the entire temperature range, expressed as:

$$T_2 = T_2^0 \exp(-E_a/RT) \quad (2)$$

where T_2^0 is the pre-exponential factor and E_a represents the apparent activation energy that describes the temperature sensitivity of T_2 (see solid lines in Fig. 2). Although the Arrhenius trend appears to hold at lower temperatures (typically below 50 °C) in hybrid hydrogels as well, T_2 clearly deviates from this behaviour at higher temperatures, indicating more complex dynamic scenarios (discussed further below). In addition, T_2 consistently decreases with increasing concentrations of CB and CMC, highlighting that although water molecules are indistinguishable in a given sample, their time-averaged dynamics are strongly influenced by the gel composition. This important finding becomes even more evident when using the alternative representation $T_2^{-1} = f(c_{CMC})$ for various x_{CB} and temperatures, which coincides with the weighted average of the relaxation rates of two fundamental water states, namely bulk and bound, expressed as

$$\frac{1}{T_2} = \phi \frac{1}{T_2^{bound}} + (1-\phi)\frac{1}{T_2^{bulk}} \quad (3)$$

where ϕ is the fraction of bound water molecules assumed to vary as c_{CMC}, resulting in $T_2^{bound} \approx 0.05$–0.1 s and $T_2^{bulk} \approx 1$–5 s regardless of the gel composition (see ESI,† Section S1).

Beyond the evolution of T_2 with the temperature and the gel formulation, it is also worth noting that E_a, extracted from Arrhenius fits between 10 °C and 50 °C, clearly decreases as either c_{CMC} or x_{CB} increases. Its values range from *ca.* 19 kJ mol^{-1} in the most dilute samples (*e.g.*, CMC0.01–, CMC0.1– and CMC-0.5–CB0), to nearly 0 kJ mol^{-1} in the densest hydrogel (CMC3–CB8), where T_2 no longer seems to depend on temperature. Although it might be tempting to link these activation energies to effective binding energies determined in rheology,[47] the interpretation in NMR is quite the opposite. Here, a low activation energy corresponds to high thermal stability in a material where water molecules move through a dense network with slow polymer dynamics.[45] While a quantitative correlation between E_a and the network density/topology remains elusive, comparing these values with rheological properties allows us to build a remarkable phase diagram presented in Fig. 3. This diagram integrates (i) the sample rheological state – either viscoelastic liquid, polymer gel, or colloidal gel, as defined above in the introduction (data extracted from ref. 18) – and (ii) the E_a values

Published on 06 November 2024. Downloaded on 29/1/2026 11:08:33 AM.

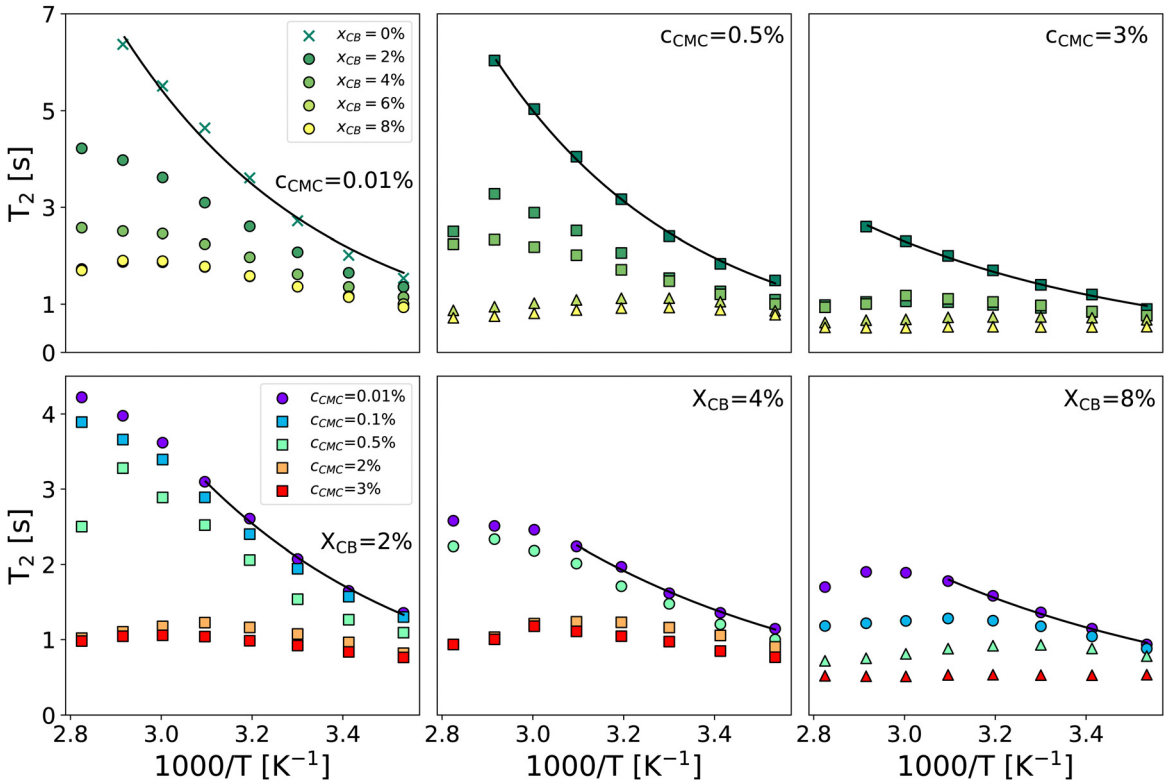

Fig. 2 Spin–spin relaxation time T_2 *vs.* reciprocal temperature for selected formulations varying x_{CB} between 0 and 8 wt% for c_{CMC} = 0.01, 0.5, and 3 wt% (top row, left to right) and varying c_{CMC} between 0.01 and 3 wt% for x_{CB} = 2, 4, and 8 wt% (bottom row, left to right). Solid lines are Arrhenius fits of data in the whole temperature range (top row) and the 283–323 K range (bottom row). Symbols refer to the rheological behavior: circle and cross: viscoelastic liquid, square: colloidal gel, and triangle: polymer gel (see the diagram in Fig. 3).

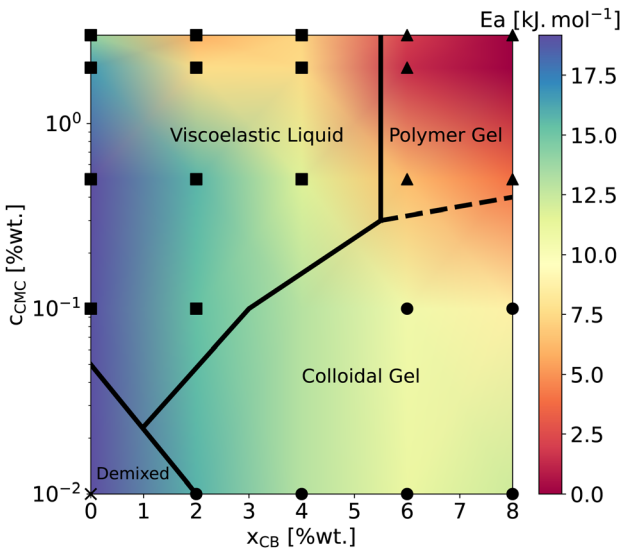

Fig. 3 Phase diagram gathering rheological state determined at T = 22 °C extracted from ref. 18 and low-temperature apparent activation energies reported in Fig. 2. Symbols mark the sample formulations investigated in the present work. Squares, triangles, circles, and crosses correspond to viscoelastic liquids, polymer gels, colloidal gels, and a CB-free polymer solution, respectively. The color map is interpolated using the Gouraud shading from the matplotlib package (Python). E_a values are reported in ESI,† Section S2.

measured from NMR experiments (see the color map). This dual analysis clearly illustrates the above-mentioned trend, showing that E_a decreases with increasing CB or CMC content, and highlights the excellent agreement between the two techniques in defining the polymer gel domain, which encompasses the densest materials (red zone). In addition, the highest E_a values (purple zone) are only observed in CB-free hydrogels, whereas nearly CMC-free gels display intermediate values (light green) across a wide range of x_{CB}, indicating that the impact of CB and CMC on E_a is not equivalent. This observation supports the correlation between macroscopic rheological properties and local water diffusion: a CB-free liquid-like sample containing a relatively high fraction of (partly hydrophilic) CMC results in a lower impact on E_a than a gel made of a small fraction (*e.g.*, 0.01 wt%) of CMC decorating a physically cross-linked network of (hydrophobic) CB particles. In other words, T_2 is more sensitive to the presence of a 3D network (even if loose and made of strands that do not interact with water molecules) than to an increase in the concentration of a polymer that interacts favorably with water in solution. Although not directly comparable, this result aligns with observations in polymer melts, where T_2 decreases with increasing cross-link density in a nearly identical chemical environment.[48] The situation becomes more complex when moving away from the left- and bottom-axes of the diagram, where it appears that CMC and CB interact synergistically to

 This journal is © The Royal Society of Chemistry 2025

Published on 06 November 2024. Downloaded on 29/1/2026 11:08:33 AM.

influence E_a. This translates into the centro-symmetric color gradient originating from the CMC3–CB8 formulation (top-right corner of the diagram). In this region, which includes the densest viscoelastic liquids and colloidal gels, as well as all the polymer gels, E_a values progressively decrease as the material densifies, regardless of whether CB or CMC concentrations are increased. The transition from colloidal gel to viscoelastic liquid implies, in this case, a decrease of E_a (see *e.g.*, x_{CB} = 4 wt%), suggesting that favorable CMC–water interactions dominate the gelation process.

Beyond the low-temperature regime mainly described by the phase diagram, a closer look at high-temperature data in Fig. 2 reveals a striking non-monotonic evolution of T_2 in several formulations, particularly noticeable for x_{CB} = 4 wt%. Overall, increasing the gel density systematically results in a progressive transition of $T_2(T)$ from (i) a monotonic Arrhenius profile, to (ii) a monotonic non-Arrhenius profile, and then to (iii) a non-monotonic profile (see *e.g.*, the c_{CMC} = 0.01% panel). While an Arrhenius profile is commonly expected from water molecules that steadily gain mobility with increasing temperature,[49] a non-monotonic evolution here suggests a thermally induced modification of the network structure. Such a modification can be attributed to a change in the conformation of CMC polymers, which form a percolated network of increasing connectivity for higher temperatures, even in the absence of CB particles.[45] This is further confirmed by CPMG experiments performed upon cooling, which show a perfect overlap of T_2 during heating and cooling for samples with an Arrhenius profile, while revealing a significant decrease in T_2 in the cooling branch for other profiles (see ESI,† Section S3). Interestingly, this hysteresis becomes more pronounced in samples with higher CB content, suggesting that denser colloid-polymer hydrogels exhibit a stronger tendency to age with changes in temperature. Although the low E_a values make it challenging to observe the non-monotonic trend of T_2 in dense gels, this observation indicates that the rheological properties of these materials are likely to evolve in a complex manner upon heating.

In line with this reasoning, Fig. 4 shows the frequency dependence of the storage modulus of CMC3–CB8 measured on three different samples at 10 °C, 50 °C, and 70 °C. All three spectra exhibit a low-frequency plateau, which is linked to the topological density of the gel through entropic elasticity,[50] and a high-frequency power-law evolution with an exponent α, corresponding to the relaxation modes of the network strands. As expected, increasing the temperature from 10 °C to 50 °C accelerates the strand relaxation dynamics and decreases the lifetime of attractive interactions ("stickers"),[51] resulting in a significant decrease of G' at both high- and low-frequencies. However, at 70 °C, the situation is more intriguing. Indeed, at this temperature, the plateau modulus increases significantly (by a factor of 4), and the power-law exponent α shifts from the Rouse-like value of 0.5 (observed for 10–50 °C) to 0.3, both of which unambiguously indicate a strong densification of the network, in good agreement with the aforementioned NMR results showing a decrease of T_2. For completeness, we also confirm that the aging kinetics vary significantly with the

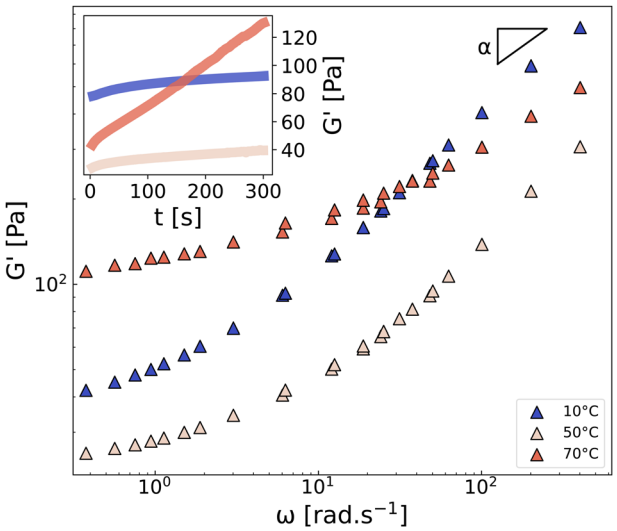

Fig. 4 Frequency dependence of the storage modulus G' of the CMC3–CB8 sample measured at 10, 50, and 70 °C for γ = 0.1%. The parameter α is the exponent characterizing the high-frequency power-law response $G' \sim \omega^{\alpha}$. Inset: Time sweep measurement performed at $\omega = 2\pi$ rad s^{-1}. See ESI,† Section S4 for G''.

temperature (see inset in Fig. 4), resulting in a rapid increase of G' at 70 °C. This observation is in line with the non-monotonic onset of T_2 observed in most formulations, from $1000/T \approx 3.0$ (*i.e.*, $T > 50$ °C) in Fig. 2, which suggests a change in the network microstructure, and therefore different aging processes and dynamics.

To summarize, we have demonstrated that low-field NMR experiments that measure the spin–spin relaxation time T_2 using the CPMG pulse sequence, are effective in probing the gelation and structural evolution of polymer–colloid hydrogels. Specifically, when using CMC, we observed a single and unstretched exponential decay of the transverse magnetization across all gel formulations and temperatures, indicating that water molecules are indistinguishable at the T_2 timescale (4 s ± 3 s for all the samples). For $T < 50$ °C, $T_2(T)$ allows for extracting an apparent activation energy E_a, which can be directly compared to rheological data, offering an alternative perspective to study gelation. In the loosest networks, E_a is about 19 kJ mol^{-1}, but it decreases to 0 kJ mol^{-1} in the densest networks, indicating a temperature-independent NMR response. On the other hand, for $T > 50$ °C, we observed significant network densification and accelerated aging, emphasizing the dominance of CB–CMC interactions over CMC–water and CMC–CMC interactions. These findings are supported by rheological experiments, establishing NMR relaxometry as a practical and valuable tool for systematically investigating hydrogels from the solvent point of view. Perspectives to improve this rheology-NMR dual approach will include systematic measurements of the spin–lattice relaxation time T_1,[52] which we expect to be much larger than T_2 due to the exchange dynamics of water molecules. Pulse-field gradient NMR methods will also be considered to quantify the fraction and the diffusion coefficient of bound molecules in denser gels.[53]

Published on 06 November 2024. Downloaded on 29/1/2026 11:08:33 AM.

Experimental section

Sample preparation

Samples are prepared by first dissolving sodium carboxymethylcellulose (NaCMC, Sigma Aldrich), M_w = 250 kg mol^{-1} and DS = 0.9 as specified by the manufacturer, (see ref. 45 for actual measured values) in deionized water (H_2O). Stock solutions up to 5 wt% are prepared and stirred at room temperature for 48 h until homogeneous, before adding the carbon black (CB) particles (VXC72R, Cabot). Samples are placed in a sonicator bath for two rounds of 90 min separated by a period of 24 h under mechanical stirring. The samples are finally left at rest for another 24 h before being tested. The samples are characterized by their CMC concentration c_{CMC} expressed in wt% of the stock solution (without CB) and their mass fraction of CB x_{CB}, following ref. 54.

LF-NMR

The ^{1}H low-field NMR experiments were performed on a Bruker minispec mq20 spectrometer (''NF'' electronics) operating at a resonance frequency of 20 MHz with 90° and 180° pulse lengths of 2.2 ms and 4.8 ms, respectively, and a dead time of 15 μs. A Car–Purcell–Meiboom–Gill (CPMG) echo train acquisition was used to measure data up to about three times the spin–spin relaxation time T_2 of the gels. The echo-time was systematically set to 2τ = 2 ms. It was varied down to 2τ = 0.25 ms for a single sample (CMC2–CB2) at 10 °C and 80 °C showing no and little effect on the measurements of T_2, respectively (see ESI,† Section S5). Measurements were performed by increasing the temperature in a step-wise manner from 10 °C to 80 °C every 10 °C with a BVT 3000 heater connected to a liquid nitrogen Dewar. Before each measurement, the temperature was left to stabilize for 10 min. For some samples, the experiments were then repeated from high to low temperatures to investigate aging effects (see ESI,† Section S3).

Rheology

The rheological properties were measured with a cone-and-plate geometry (angle 2°, radius 20 mm and truncation 46 μm) connected to a strain-controlled rheometer (ARES G2, TA Instruments). The cone was smooth and the plate was sand-blasted with a surface roughness of about 1 μm to prevent wall slip. For a given sample, each temperature was probed independently with a different loading and independent gap calibration. The three temperatures probed T = 10, 50, and 70 °C were maintained constant by a Peltier modulus placed under the bottom plate. The rheological protocol for linear viscoelastic characterization of the samples was divided into three consecutive steps: (i) a preshear at $\dot{\gamma}$ = 500 s^{-1} for 3 min to erase the loading history and rejuvenate the sample;[55–57] (ii) a recovery phase of 5 min during which we monitored the sample linear viscoelastic properties by applying small amplitude oscillations in the linear regime at a frequency $\omega = 2\pi$ rad s^{-1}; (iii) a frequency sweep performed by mutliwave strain signals[58] in the linear regime to span frequencies from ω = 0.30 to 420 rad s^{-1}. The samples remained in the rheometer for 9 minutes, and no evidence of alternation due to evaporation was witnessed by visual inspection, even at the highest temperature.

Author contributions

CRediT: Léo Hervéou conceptualization, data curation, formal analysis, investigation, methodology, software, visualization, writing – review & editing; Gauthier Legrand conceptualization, investigation, validation, writing – review & editing; Thibaut Divoux conceptualization, methodology, project administration, resources, supervision, visualization, validation, writing – original draft, writing – review & editing; Guilhem P. Baeza conceptualization, methodology, project administration, resources, supervision, visualization, validation, writing – original draft, writing – review & editing.

Data availability

Data for this article, including CPMG measurements $I(t)$ for all the samples are available at **https://www.researchgate.net/publication/384054735_Herveou_et_al_CPMG**, DOI: **https://doi.org/10.13140/RG.2.2.30502.33604**.

Conflicts of interest

There are no conflicts to declare.

Acknowledgements

All the authors warmly thank Carlos Fernandez-de-Albá (IMP, INSA-Lyon) and Cédric Lorthioir (LCMCP, Sorbonne University, Paris) for technical support and insightful discussions about low-field NMR experiments. This work was supported by the LABEX iMUST of the University of Lyon (ANR-10-LABX-0064), created within the ''Plan France 2030'' set up by the French government and managed by the French National Research Agency (ANR).

Notes and references

1 E. A. Appel, J. del Barrio, X. J. Loh and O. A. Scherman, *Chem. Soc. Rev.*, 2012, **41**, 6195–6214.
2 J. P. Gong, *Soft Matter*, 2010, **6**, 2583–2590.
3 Q. Chen, H. Chen, L. Zhu and J. Zheng, *J. Mater. Chem. B*, 2015, **3**, 3654–3676.
4 X. Li and J. P. Gong, *Nat. Rev. Mater.*, 2024, 1–19.
5 R. Messing and A. M. Schmidt, *Polym. Chem.*, 2011, **2**, 18–32.
6 J. Li, W. R. Illeperuma, Z. Suo and J. J. Vlassak, *ACS Macro Lett.*, 2014, **3**, 520–523.
7 X. Li, C. Tang, D. Liu, Z. Yuan, H.-C. Hung, S. Luozhong, W. Gu, K. Wu and S. Jiang, *Adv. Mater.*, 2021, **33**, 2102479.
8 H. Zhang, F. Zhang and R. Yuan, *Hydrogels based on natural polymers*, Elsevier, 2020, pp. 357–410.
9 P. C. Nath, S. Debnath, K. Sridhar, B. S. Inbaraj, P. K. Nayak and M. Sharma, *Gels*, 2022, **9**, 1.

 This journal is © The Royal Society of Chemistry 2025

Published on 06 November 2024. Downloaded on 29/1/2026 11:08:33 AM.

10 S. Rose, A. Prevoteau, P. Elzière, D. Hourdet, A. Marcellan and L. Leibler, *Nature*, 2014, **505**, 382–385.
11 R. V. Ulijn, N. Bibi, V. Jayawarna, P. D. Thornton, S. J. Todd, R. J. Mart, A. M. Smith and J. E. Gough, *Mater. Today*, 2007, **10**, 40–48.
12 L. L. Palmese, R. K. Thapa, M. O. Sullivan and K. L. Kiick, *Curr. Opin. Chem. Eng.*, 2019, **24**, 143–157.
13 F. Zhao, J. Bae, X. Zhou, Y. Guo and G. Yu, *Adv. Mater.*, 2018, **30**, 1801796.
14 Y. Shi, L. Peng and G. Yu, *Nanoscale*, 2015, **7**, 12796–12806.
15 P. Schexnailder and G. Schmidt, *Colloid Polym. Sci.*, 2009, **287**, 1–11.
16 H. Dehne, F. Hecht and A. Bausch, *Soft Matter*, 2017, **13**, 4786–4790.
17 C. Y. Anthony, A. A. Smith and E. A. Appel, *Mol. Syst. Des. Eng.*, 2020, **5**, 401–407.
18 G. Legrand, S. Manneville, G. H. McKinley and T. Divoux, *Macromolecules*, 2023, **56**, 2298–2308.
19 R. Moakes, A. Sullo and I. Norton, *Food Hydrocoll.*, 2015, **45**, 227–235.
20 C. Tanford, *Adv. Protein Chem.*, 1968, **23**, 121–282.
21 R. Fan, Y. Cheng, R. Wang, T. Zhang, H. Zhang, J. Li, S. Song and A. Zheng, *Polymers*, 2022, **14**, 2379.
22 S. C. Deoni, *Magn. Reson. Neuroimag.*, 2011, 65–108.
23 C. Granziera and T. Sprenger, Brain Inflammation, Degeneration, and Plasticity in Multiple Sclerosis, in *Brain Mapping*, ed. A. W. Toga, Academic Press, Waltham, 2015, pp. 917–927.
24 T. Salomonsen, M. T. Sejersen, N. Viereck, R. Ipsen and S. B. Engelsen, *Int. Dairy J.*, 2007, **17**, 294–301.
25 N. Harbourne, J. C. Jacquier and D. ORiordan, *Int. Dairy J.*, 2011, **21**, 185–191.
26 E. Kirtil and M. H. Oztop, *Food Eng. Rev.*, 2016, **8**, 1–22.
27 B. Ozel, S. S. Uguz, M. Kilercioglu, L. Grunin and M. H. Oztop, *J. Food Process Eng.*, 2017, **40**, e12465.
28 K.-F. Ratzsch, C. Friedrich and M. Wilhelm, *J. Rheol.*, 2017, **61**, 905–917.
29 N. W. Radebe, K.-F. Ratzsch, C. O. Klein and M. Wilhelm, *Rheol. Proc. Construct. Mater.*, 2020, **2**, 256–265.
30 C. Fengler, J. Keller, K.-F. Ratzsch and M. Wilhelm, *Adv. Sci.*, 2022, **9**, 2104231.
31 Y. Xiong, Z. Xia, A. Lu and W. Chen, *Anal. Chem.*, 2023, **95**, 7545–7551.
32 B. Maillet, R. Sidi-Boulenouar and P. Coussot, *Langmuir*, 2022, **38**, 15009–15025.
33 H. Y. Carr and E. M. Purcell, *Phys. Rev.*, 1954, **94**, 630.
34 S. Meiboom and D. Gill, *Rev. Sci. Instrum.*, 1958, **29**, 688–691.
35 R. W. Brown, Y.-C. N. Cheng, E. M. Haacke, M. R. Thompson and R. Venkatesan, *Magnetic resonance imaging: physical principles and sequence design*, John Wiley & Sons, 2014.
36 G. D. Fullerton, J. L. Potter and N. C. Dornbluth, *Magn. Reson. Imaging*, 1982, **1**, 209–226.
37 D. Besghini, M. Mauri, P. Hashemi, M. Knarr, R. Adden, P. Mischnick and R. Simonutti, *Macromolecules*, 2023, **56**, 4694–4704.
38 D. Capitani, V. Crescenzi, A. De Angelis and A. Segre, *Macromolecules*, 2001, **34**, 4136–4144.
39 M. Abrami, G. Chiarappa, R. Farra, G. Grassi, P. Marizza and M. Grassi, *ADMET DMPK*, 2018, **6**, 34–46.
40 P. Y. Ghi, D. J. Hill and A. K. Whittaker, *Biomacromolecules*, 2002, **3**, 991–997.
41 M. Kanekiyo, M. Kobayashi, I. Ando, H. Kurosu, T. Ishii and S. Amiya, *J. Mol. Struct.*, 1998, **447**, 49–59.
42 M. Abrami, I. DAgostino, G. Milcovich, S. Fiorentino, R. Farra, F. Asaro, R. Lapasin, G. Grassi and M. Grassi, *Soft Matter*, 2014, **10**, 729–737.
43 M. Abrami, F. Bignotti, F. Baldi, G. Spagnoli, A. Biasin, L. Grassi, G. Grassi and M. Grassi, *Int. J. Pharm.*, 2023, **637**, 122882.
44 J. H. Wang, *J. Phys. Chem.*, 1965, **69**, 4412.
45 G. Legrand, G. P. Baeza, S. Manneville and T. Divoux, *arXiv*, 2024, preprint, arXiv:2406.04453, DOI: 10.48550/arXiv.2406.04453.
46 G. Legrand, G. P. Baeza, M. Peyla, L. Porcar, C. Fernandez-de Alba, S. Manneville and T. Divoux, *ACS Macro Lett.*, 2024, **13**, 234–239.
47 G. P. Baeza, C. Dessi, S. Costanzo, D. Zhao, S. Gong, A. Alegria, R. H. Colby, M. Rubinstein, D. Vlassopoulos and S. K. Kumar, *Nat. Commun.*, 2016, **7**, 11368.
48 V. Litvinov, W. Barendswaard and M. Van Duin, *Rubber Chem. Technol.*, 1998, **71**, 105–118.
49 M. Sattig, S. Reutter, F. Fujara, M. Werner, G. Buntkowsky and M. Vogel, *Phys. Chem. Chem. Phys.*, 2014, **16**, 19229–19240.
50 L. R. G. Treloar, *The physics of rubber elasticity*, OUP Oxford, 1975.
51 L. Leibler, M. Rubinstein and R. H. Colby, *Macromolecules*, 1991, **24**, 4701–4707.
52 C. D'Agostino, R. Liuzzi, L. F. Gladden and S. Guido, *Soft Matter*, 2017, **13**, 2952–2961.
53 C. DAgostino, V. Preziosi, G. Caiazza, M. V. Maiorino, E. Fridjonsson and S. Guido, *Soft Matter*, 2023, **19**, 3104–3112.
54 G. Legrand, S. Manneville, G. H. McKinley and T. Divoux, *Macromolecules*, 2023, **56**, 2298–2308.
55 V. Viasnoff and F. Lequeux, *Phys. Rev. Lett.*, 2002, **89**, 065701.
56 D. Bonn, M. M. Denn, L. Berthier, T. Divoux and S. Manneville, *Rev. Mod. Phys.*, 2017, **89**, 035005.
57 Y. M. Joshi and G. Petekidis, *Rheol. Acta*, 2018, **57**, 521–549.
58 M. Mours and H. H. Winter, *Rheol. Acta*, 1994, **33**, 385–397.